Measurement of Heteronuclear Bond Distances in Polycrystalline Solids by Solid-State NMR Techniques

James E. Roberts,† Gerard S. Harbison,‡ Michael G. Munowitz,§ Judith Herzfeld,⊥ and Robert G. Griffin*

Contribution from the Francis Bitter National Magnet Laboratory, Massachusetts Institute of Technology, Cambridge, Massachusetts 02139, Department of Physiology and Biophysics, Harvard Medical School, Boston, Massachusetts 02115, and Amoco Research Center, Naperville, Illinois 60566. *Received June 25, 1986*

Abstract: High resolution dipolar/chemical shift NMR experiments for solids are critically reviewed and used to measure $^{15}N-^{1}H$ bond distances in a series of compounds, many of which have also been studied by neutron diffraction. The results demonstrate that when recorded carefully, with attention paid to the experimental procedures described, two-dimensional dipolar/chemical shift spectra can yield bond distances accurate to within 0.005 Å and mutual orientations of dipolar and chemical shift tensors accurate to within 3°. A comparison of the NMR distances with similar data from neutron diffraction experiments shows the NMR distances to be uniformly ~0.035 Å longer, a result that is consistent with some vibrational averaging of the $^{15}N-^{1}H$ dipolar interaction. Collectively, the experimental data and procedures described here demonstrate for the first time that high resolution dipolar/chemical shift NMR experiments are a viable method for locating protons in polycrystalline or amorphous solids. Previously, such determinations have been possible only with single crystal neutron diffraction techniques.

Magnetic dipolar fields produced by ^{1}H nuclei figure prominently in almost all solid-state NMR experiments designed for spin $^{1}/_{2}$ systems, where they create both obstacles and opportunities for high-resolution spectroscopy. On the one hand, the spread of resonant frequencies that results from the existence of relatively strong anisotropic magnetic fields in the sample inevitably broadens, and sometimes obscures, the response of all the nuclei within; on the other hand, a spectrum obtained in the presence of such a local field is rich with details of molecular structure, owing to the well-known dependence of the dipole–dipole interaction on internuclear distances and angles. The measurement of nuclear magnetic dipole–dipole couplings therefore provides a straightforward means of ascertaining molecular geometry in the solid state, at least in principle. In practice, however, the local field is frequently too complex to yield to a detailed analysis, so it is perhaps not surprising that most solid-state NMR spectra are recorded with pulse sequences and conditions designed to attenuate dipolar couplings in favor of single-spin chemical shift interactions.

This philosophy underlies the method of dilute-spin double resonance, whereby the heteronuclear coupling is exploited as a thermal conduit for polarization transfer from a subsystem of abundant ^{1}H nuclei to a subsystem of magnetically dilute spin $^{1}/_{2}$ species, but then is removed entirely while the enhanced response of the rare spins is observed.[1] The basic tools of Hartmann–Hahn cross-polarization (CP)[2] and proton decoupling, together with magic-angle sample spinning (MASS),[3-5] are now employed routinely to yield well-resolved, chemically shifted spectra of ^{13}C, ^{15}N, ^{29}Si, and ^{31}P. This approach is equally applicable to other isotopes for which the homonuclear dipolar coupling is already weak as a result of low natural abundance, large internuclear separations, small magnetic moments, or any combination of these factors. Concurrently, new approaches capable of producing high resolution dipolar spectra and thus restoring the previously discarded information concerning molecular structure have also been developed. In this broad class of methods are techniques such as zero-field spectroscopy,[6] under which the spatial anisotropy of the dipolar interaction is removed; nutation spectroscopy,[7] applicable mostly to dilute homonuclear pairs; and dipolar/chemical shift spectroscopy, a family of two-dimensional experiments used to separate these two interactions in spectra of solids.[8-15]

Perhaps the most generally useful and versatile approach to dipolar spectroscopy is offered by the experiment employing both MASS and 2D dipolar/chemical shift spectroscopy.[10-13] Applicable to the same dilute heteronuclear spin $^{1}/_{2}$ systems in which cross-polarization is most favorable, these methods seek to measure the local magnetic dipolar field at every chemically inequivalent site in a system, and to relate this field directly to the number, kind, and arrangement of neighboring nuclei from which it arises. Typically, the rare spin S is found near one or more abundant spins I, usually protons. Whether or not the goal of clean local field separation is realized depends upon the extent to which signals from the chemically inequivalent S nuclei are resolved and upon the extent to which the sources of the local field, the I nuclei, are restricted to a manageable number. The resolution needed to satisfy the first requirement is obtained most effectively with the aid of MASS, which disentangles overlapping local field spectra from the various sites; the simplification needed to satisfy the second requirement is achieved both by exploiting the rapid diminution of the dipolar interaction with increasing internuclear separation and by manipulating the spin dynamics to suppress the

* Massachusetts Institute of Technology.
† Massachusetts Institute of Technology. Present address: Department of Chemistry, Lehigh University, Bethlehem, PA 18015.
‡ Harvard Medical School. Present address: Department of Chemistry, State University of New York at Stony Brook, Stony Brook, NY 11794.
§ Amoco Research Center.
⊥ Harvard Medical School. Present address: Department of Chemistry, Brandeis University, Waltham, MA 02154.

(1) Pines, A.; Gibby, M.; Waugh, J. S. *J. Chem. Phys.* **1973**, *59*, 569.
(2) Hartmann, S.; Hahn, E. L. *Phys. Rev.* **1962**, *128*, 2042.
(3) Lowe, I. J. *Phys. Rev. Lett.* **1959**, *2*, 285.
(4) Andrew, E. R.; Bradbury, A.; Eades, R. G. *Nature (London)* **1958**, *182*, 1659.
(5) Schaefer, J. F.; Stejskal, E. O. *J. Am. Chem. Soc.* **1976**, *98*, 1031.
(6) Zax, D. B.; Bielecki, A.; Zilm, K. W.; Pines, A.; Weitekamp, D. P. *J. Chem. Phys.* **1985**, *83*, 4877.
(7) Yannoni, C. S.; Clarke, T. C. *Phys. Rev. Lett.* **1983**, *51*, 1191. Yannoni, C. S.; Kendrick, R. D. *J. Chem. Phys.* **1981**, *74*, 747.
(8) Hester, R. K.; Ackerman, J. L.; Neff, B. L.; Waugh, J. S. *Phys. Rev. Lett.* **1976**, *36*, 1081.
(9) Stoll, M. E.; Vega, A. J.; Vaughan, R. W. *J. Chem. Phys.* **1976**, *65*, 4093.
(10) Munowitz, M. G.; Griffin, R. G.; Bodenhausen, G.; Huang, T. H. *J. Am. Chem. Soc.* **1981**, *103*, 2529.
(11) Munowitz, M. G.; Griffin, R. G. *J. Chem. Phys.* **1982**, *76*, 2848; *77*, 2217.
(12) Munowitz, M. G.; Aue, W. P.; Griffin, R. G. *J. Chem. Phys.* **1982** *77*, 1686.
(13) Munowitz, M. G.; Griffin, R. G. *J. Chem. Phys.* **1983**, *78*, 613.
(14) DiVerdi, J. A.; Opella, S. J. *J. Am. Chem. Soc.* **1982**, *104*, 1761.
(15) Linder, M.; Hohener, A.; Ernst, R. R. *J. Chem. Phys.* **1980**, *73*, 4959.

0002-7863/87/1509-4163$01.50/0

homonuclear I–I couplings. When all these conditions are met, the spectrum that results supplies not only the three principal values of the chemical shift anisotropy (which, of course, are available from the simple MASS spectrum described above), but also the orientation of the chemical shift tensor in the molecular framework and the principal values of the dipolar coupling tensor as well.[11-12] An analysis of these coupling constants, based solely upon internuclear distances and angles, then provides a picture of the local structure and dynamics at each site.

Although many of the theoretical features of the MASS dipolar/chemical shift experiment have been discussed at length in previous papers[10-13], there has not yet been a careful experimental investigation demonstrating that the method can yield accurate and precise bond distance information. Indeed, in most of the data published thus far, the measured NMR bond distances are anomalously long when compared to diffraction data, and there has not been a fully satisfactory explanation for this discrepancy.[12,14] In this article we focus on the technical requirements that must be observed to obtain accurate, reproducible data from polycrystalline or amorphous solid samples. Appearances to the contrary notwithstanding, the experiment is relatively easy to perform, and it can yield proton–rare spin bond distances with precision better than 0.5% when carefully adjusted. Since these quantities are otherwise accessible only through neutron diffraction studies of single crystals, and since the location of protons is crucial in a variety of chemical, physical, and biological problems, the eventual reward is great compared to the surprisingly modest experimental and computational efforts required. With this end in mind, following a review of the theoretical foundations supporting the experimental design, we discuss those features of the method that are essential for its successful implementation. Supporting this discussion and illustrating the chemical value of high-resolution dipolar spectra is a set of six ^{15}N–^{1}H bond distances in which variations as small as 0.01 Å are readily discernible. Many of the compounds chosen for these studies have also been examined with neutron diffraction, so it is possible to compare data from the two techniques. For these particular AX spin systems bond distances measured by NMR are about 0.035 Å longer than those measured by neutron diffraction. We believe this difference is a genuine effect and is due to vibrational averaging of the NMR spectra.

Theoretical Background

The energy levels of a dilute spin S near N abundant nuclei I_1, I_2...I_n are determined largely by the Hamiltonian

$$\mathcal{H} = H_S + H_{IS} + H_{II} \quad (1)$$

a combination of chemical shift and direct spin–spin couplings. Indirect J couplings are usually small enough relative to the dipole–dipole interactions to neglect initially.

The first term of the simplified Hamiltonian

$$H_S = [\sigma + \sigma_{zz}\{(3\cos^2\theta - 1) + \eta \sin^2\theta \cos 2\phi\}/2]S_z \quad (2)$$

expresses the anisotropic chemical shift interaction in terms of the isotropic trace $\sigma = (\sigma_{xx} + \sigma_{yy} + \sigma_{zz})/3$, the shielding anisotropy σ_{zz}, the asymmetry parameter $\eta = (\sigma_{xx} - \sigma_{yy})/(\sigma_{zz} - \sigma)$, and the polar coordinates (θ,ϕ) of the external magnetic field in the principal axis system $\sigma(xyz)$.

The truncated heteronuclear interaction

$$H_{IS} = -\sum_{i=1}^{N} 2D_{iS}I_{zi}S_z \quad (3)$$

where

$$D_{iS} = \gamma_I\gamma_S\hbar\{(3\cos^2\theta_{iS} - 1)/2r_{iS}^3\} \quad (4)$$

gives the coupling of the S spin with the quasistatic local field of each I spin as a function of the magnitude and orientation of each internuclear vector r_{iS}. The homonuclear interaction

$$H_{II} = -\sum_{i<j} D_{ij}(3I_{zi}I_{zj} - \vec{I}_i\cdot\vec{I}_j) \quad (5)$$

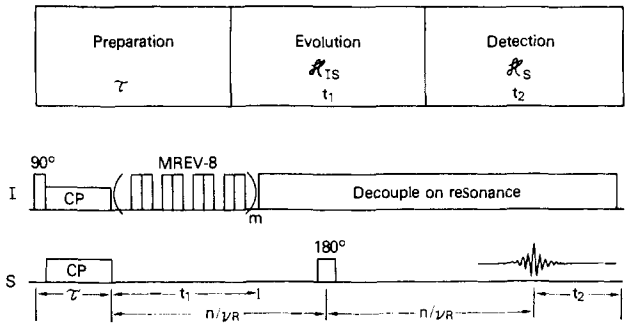

Figure 1. General two-dimensional dipolar/chemical shift pulse sequence used to obtain heteronuclear bond distances. The timing of some pulses is synchronized with the rotor period as indicated. If only a single isotropic chemical shift is present, the 180° pulse is not required, and data acquisition commences at any rotational echo.

allows for flip-flops among the abundant spins, under which only the total angular momentum component

$$I_z = \sum_{i=1}^{N} I_{zi} \quad (6)$$

is conserved. If H_{II} is absent, however, the individual Zeeman components m_i become good quantum numbers, and a simple local field picture prevails. In these circumstances the S spin, excited by a $\pi/2$ pulse or its equivalent, evolves under H_{IS} as

$$\langle S_x(t_1)\rangle = \langle S_x(0)\rangle \prod_{i=1}^{N} \cos(D_{iS}t_1) \quad (7)$$

so that its transverse magnetization component oscillates at frequencies given by all possible arithmetic combinations of the local fields of the I spins. Hence when only one I spin is near the S nucleus, the heteronuclear S dipolar spectrum is dominated by the largest coupling and splits into a doublet in accord with the two allowed values of m_i. Smaller interactions with distant I nuclei add a dense fine structure to the energy levels, splitting and resplitting the resonance and thus imparting a finite line width to each component of the doublet.

Spectroscopic separation of the dipolar and chemical shift interactions is usually accomplished with a two-dimensional pulse sequence of the sort diagrammed in Figure 1. The experiment begins with an excitation period τ during which transverse magnetization S_x is created. Hartmann–Hahn cross-polarization techniques frequently are employed during this interval, but the experimental design need not presuppose any particular method of excitation. The first response period, t_1, is allocated entirely to the heteronuclear Hamiltonian H_{IS}: chemical shifts are removed by spin-echo techniques, and homonuclear dipole–dipole interactions are attenuated by the application of a multiple-pulse line-narrowing sequence to the I spins. Under these conditions, the evolution of the system theoretically is governed by the scaled heteronuclear coupling

$$H_{IS} = -\sum_{i=1}^{N} K(2D_{iS}I_{zi}S_z) \quad (8)$$

where the scaling factor K depends on the form of the multiple-pulse sequence used to suppress the homonuclear interactions. Whether or not the idealized local field picture is realized experimentally is determined primarily by the performance of the line-narrowing sequence. Accurate interpretation of the resulting dipolar spectrum also depends on the prior measurement of K under the exact experimental conditions used during the local field measurements.

Following the dipolar evolution period is a second response period, t_2, throughout which only the chemical shift interactions described by H_S are present. A conventional proton-decoupled signal is recorded during this interval for each value of t_1. Double Fourier transformation of the data matrix, $S(t_1,t_2)$, produces a two-dimensional spectrum, $S(\omega_1,\omega_2)$, in which the dipolar frequencies appear parallel to the axis ω_1 and the chemical shift

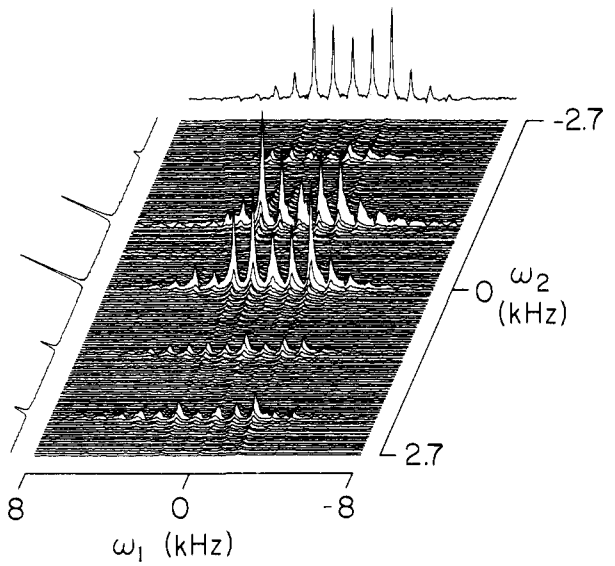

Figure 2. Two-dimensional ^{15}N–^{1}H dipolar/chemical shift spectrum obtained from [^{15}N]acetylvaline showing the dipolar and chemical shift projections. Line widths are typically 50–150 Hz for the dipolar and 0.5–1.0 ppm for the chemical shift dimension. ν_R = 1.07 kHz.

frequencies appear parallel to the axis ω_2.

The dipolar/chemical shift experiment described above works well for single crystals, where there exist only a few distinct orientations of the dipolar and chemical shift principal axes relative to the laboratory frame.[8] When polycrystalline or amorphous samples are used, however, the spectra arising from both H_{IS} and H_S are inhomogeneously broadened into powder patterns by the orientational disorder, and the complexity of the two-dimensional spectrum increases accordingly.[15] Overlap between signals originating from chemically inequivalent S species compounds the difficulty. Despite these complications, informative local field spectra of powder samples may be obtained if MASS is used to narrow each broad anisotropy pattern into a sharp centerband flanked by rotational sidebands. Under these conditions the Hamiltonian acquires an explicit time dependence, and the products of frequency and time in eq 7 above are replaced by time integrals. The sidebands develop from the periodic modulation of the internal interactions.[11]

The beneficial effects of sample spinning are evident in the two-dimensional dipolar/chemical shift stacked plot of [^{15}N]-acetylvaline shown in Figure 2. Here the Pake doublet arising from the ^{15}N–^{1}H coupling is projected onto the dipolar axis as a distribution of sidebands about $\omega_1 = 0$, and the chemical shift anisotropy pattern is similarly projected onto the orthogonal axis as another distribution of sidebands centered about the isotropic frequency $\omega_2 = \sigma$. The geometric relationship between the principal axis systems of the dipolar and chemical shift interactions determines the distribution of sideband intensity and phase in the interior of the spectrum. Thus may be extracted all the parameters pertaining to the two spin interactions, but now spectra from other sites may be interleaved between the narrow signals and studied independently in the same experiment.

Experimental Methods

A. Sample Preparation. [^{15}N]Glycine, [^{15}N]glycyl[^{15}N]glycine, L-tryptophan-[^{15}N]indole, and [^{15}N]trimethylammonium chloride were obtained from Stohler Isotope Chemicals (Waltham, MA). [^{15}N]-Acetylglycine was prepared from [^{15}N]glycine by the method of Herbst.[16] α-[^{15}N]glycyl[^{15}N]glycine·HCl and L-tryptophan·HCl were prepared by dissolving L-tryptophan and glycylglycine, respectively, in a small excess of 3 M HCl, rapidly evaporating in vacuo at 5 °C, and then recrystallizing from 0.1 M HCl. (π-^{15}N]-L-Histidine hydrochloride monohydrate was obtained by dissolving L-histidine (π-^{15}N) (the kind gift of Dr. W. Bachovchin, Tufts University) in a minimum of water at 60 °C and titrating to pH 4.5 with concentrated HCl. On cooling to 0 °C the only moderately soluble hydrochloride monohydrate precipitated: its ^{15}N chemical shift was identical with that of an unlabeled sample previously used for a single crystal study.[17] [^{15}N]Trimethylammonium iodide was obtained by adding a 100% excess of concentrated hydriodic acid to a methanol solution of trimethylamine and evaporating in vacuo: the methanolic trimethylamine itself was produced by passing a solution of the hydrochloride in methanol down a methanol-washed Dowex-1 column in the hydroxide form. All of the above samples were enriched to greater than 95% in ^{15}N.

B. NMR Measurements. All NMR spectra were obtained on a homebuilt pulse spectrometer operating at 317.7 and 32.2 MHz for protons and nitrogen-15, respectively. the maximum radio frequency field strengths were approximately 65 G for ^{15}N and 25 G for ^{1}H. Powdered samples of 100 to 150 mg were tightly packed into ceramic double bearing rotors (Doty Scientific); sample spinning rates varied from 0 kHz (i.e., a static powder pattern) to approximately 1.6 kHz. Typical cross-polarization contact times were 1.0 ms, with 5- to 60-s recycle delays between successive scans. The MREV-8 cycle time was typically 54 μs, with radio frequency pulse widths of 2.4–2.8 μs. Generally, 128 t_1 values were employed and an entire experiment required 14–17 h for completion.

C. NMR Protocols. The specific pulse sequence used to obtain the two-dimensional spectra presented in this work is diagrammed in Figure 1. Different forms of the basic experiment have been employed in this laboratory[10,12,13] and elsewhere to study dipolar and J couplings in various systems. Since the experiment is built around cross-polarization and MASS, the usual experimental procedures of dilute spin double resonance techniques must first be followed. We therefore pass over without additional comment such details as proper adjustment of the Hartmann–Hahn condition, contact time, repetition rate, and magic angle. One parameter worth mentioning explicitly, however, is the rate of rotation: this quantity must not exceed the widths of the static dipolar and chemical shift powder patterns if the anisotropic components of these interactions are to be preserved. The intentional generation of rotational sidebands is, of course, one feature that clearly distinguishes the high resolution dipolar/chemical shift experiment from the usual MASS procedure.

The pulse sequence of Figure 1 includes a π-pulse to refocus the isotropic components of the S chemical shift interaction, and thus remove frequency-dependent phase shifts from the spectrum recorded during t_2. If only one isotropic chemical shift is present, as in several of the ^{15}N-labeled materials examined here, this refocusing pulse may be omitted. Anisotropic components of H_S are effectively removed from the first response interval by setting the beginning of the detection interval, t_2 = 0, at a fixed, integral number of rotational periods. In this way the system enters the second response period with its dynamics unaffected by H_S.

The evolution period, t_1, is the key interval in the experiment and therefore must be set up with special care. We use the eight-pulse MREV-8 cycle[18] to suppress proton–proton couplings during this time since it is easy to implement and generally yields narrower lines than the four-pulse cycle WHH-4.[19] The step size Δt_1 is taken as one eight-pulse cycle t_c, so the bandwidth available for the dipolar spectrum is $\omega_1 = 1/t_c$. Should a broader spectral width be needed, t_1 may be increased by half-cycles instead of full cycles. The tune-up procedure employed for the ^{1}H multiple-pulse experiments is that suggested by Vaughan et al.[20] and described more recently by Gerstein.[21]

The performance of the multiple-pulse sequence depends critically on the amplitude and phase balance of the ^{1}H radio frequency (rf) pulses. These are adjusted first on a small spherical sample of water with use of standard procedures. The scaling factor K is measured directly on the sample of interest. Essential to the electronic configuration of the spectrometer is a mechanism whereby the observation channel can be changed from ^{1}H to the rare spin *without altering any of the ^{1}H radio frequency paths.* A completely nonperturbing interchange is actually not possible since most instruments have only one receiver, but the disturbances can be minimized nonetheless by switching the channels *after* the preamplifiers. Specifically, both preamplifiers are connected to the probe by appropriate $\lambda/4$ cables and grounded crossed diodes, and the obser-

(16) Herbst, R. M.; Shemin, D. *Organic Syntheses*; Wiley: New York, 1943; Collect. Vol. II, p 11.

(17) Harbison, G. S.; Herzfeld, J.; Griffin, R. G. *J. Am. Chem. Soc.* **1981**, *103*, 4752.

(18) Mansfield, P. *J. Phys. C.* **1971**, *58*, 1772. Rhim, W. K.; Elleman, D. D.; Vaughan, R. W. *J. Chem. Phys.* **1973**, *58*, 1772.

(19) Waugh, J. S.; Huber, L. M.; Haeberlen, U. *Phys. Rev. Lett.* **1968**, *20*, 180.

(20) Vaughan, R. W.; Elleman, D. D.; Stacey, L. M.; Rhim, W. K.; Lee, J.-W. *Rev. Sci. Instrum.* **1972**, *43*, 1356.

(21) Gerstein, B. C. *Phil. Trans. R. Soc. London* **1981**, *299*, 521.

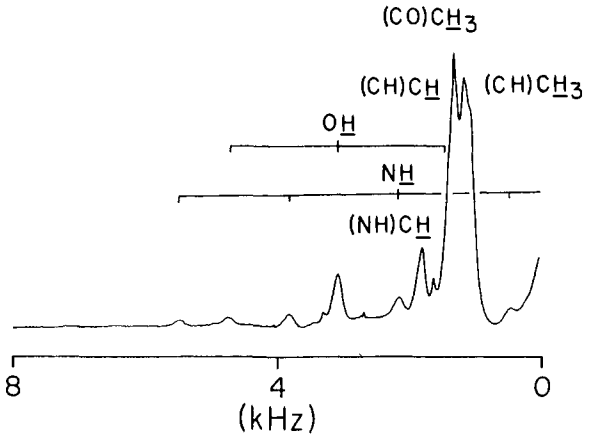

Figure 3. Proton MREV-8 multiple-pulse MASS spectrum of [^{15}N]-acetylvaline. The assignments are based on solution chemical shifts and spectra obtained at other spinning speeds. The individual line widths are ~0.9 ppm, scaled. ν_R = 1.56 kHz.

vation channel is then selected simply by exchanging a cable and a dummy load on the preamplifier outputs. It is difficult to measure the scaling factor accurately without such an arrangement, for the amplitude of the ^{1}H rf field may change by 20% if the ^{1}H preamplifier/probe interface must be disconnected to observe the ^{1}H signal.

The multiple-pulse scaling factor is obtained directly from the variation in proton chemical shift observed with changes in the proton irradiation frequency, both before and after the full two-dimensional experiment is run. The theoretical value of K for MREV-8 is 0.471, and in practice, acceptable experimental values usually fall within the range 0.460–0.480. An MREV-8 proton MASS spectrum of [^{15}N]acetyl-*d,l*-valine, shown in Figure 3, offers an example. This spectrum is admittedly unusual because the individual resonances, which are less than 1 ppm wide after scaling, are narrow enough to permit assignments to be made. Several rotational sidebands due to the ^{15}N–^{1}H dipolar coupling are also visible. Nevertheless, the general lesson to be drawn is that line positions are readily determined for most compounds, and therefore the scaling factor can be measured by observing the shifts of individual lines as the proton irradiation frequency is changed. For systems of high molecular weight, however, it may be useful to add 5–10 mg of adamantane as an internal standard for the measurement. It is also generally desirable to average at least 20 scans in order to minimize the effects of instabilities in the proton amplifier.

It must be emphasized that the MREV-8 spectrum of Figure 3 was obtained under experimental conditions as close as possible to those of the two-dimensional experiment. The pulse sequence used to measure the scaling factor begins with a cross-polarization interval before the MREV-8 train is initiated. The rf power levels and pulse lengths, recycle delay, and cross-polarization parameters are unchanged. Moreover, since the multiple-pulse spectra are best obtained off-resonance, the proton frequency is switched off-resonance during t_1 (via the remote BCD input of the frequency synthesizer) and back on-resonance when acquisition commences at the end of the t_1 interval. The performance of the multiple-pulse sequence is also degraded by residual imperfections in the rf amplitude and phase balance, which introduce an asymmetry around the carrier frequency. A line positioned on one side of the carrier may be narrower than a line in the corresponding position on the other side, even though the scaling factor is the same for both positive and negative offsets. Furthermore, a small spin-locked component along the effective field may appear as a discontinuity in the scaling factor at zero offset.[22] For these reasons the scaling factor should be measured over a 6–8-kHz range on both sides of the carrier frequency. When the shifts are measured over the entire range of resonance offsets, the correction is typically 0.01–0.02. These points are illustrated for [^{15}N]acetylvaline in Figure 4, where the "break" at zero offset is intentionally magnified by a factor of 5 in the graph.

At this point the spectrometer is switched to rare spin (^{15}N) observation and the timing of the two-dimensional experiment is determined. Here it is helpful to compare the absolute intensity of the spectrum obtained at t_1 = 0 with the absolute intensity of the spectrum obtained at $t_1 = 1/\nu_R$, the first dipolar rotational echo. The widths of the dipolar

(22) Haeberlen, U. "High Resolution NMR in Solids: Selective Averaging", *Advances in Magnetic Resonance, Supplement 1*, Academic Press New York, 1976. *Advances in Magnetic Resonance: Supplement 1*; Academic Press: New York, 1976.

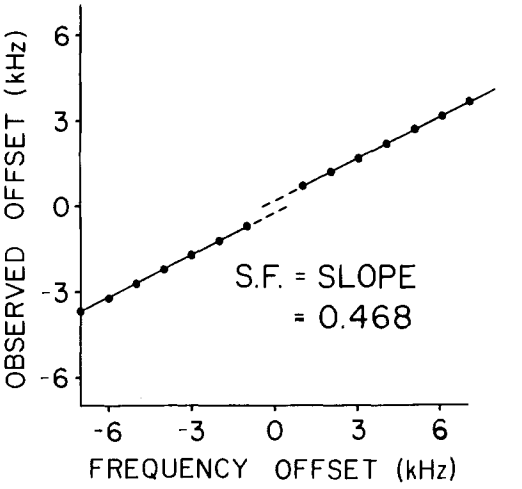

Figure 4. Plot of the observed frequency offset vs. proton irradiation offset for MREV-8 on [^{15}N]acetylvaline during MASS. The slope is equal to the multiple-pulse scaling factor. The small break at zero offset is due to small imperfections in the pulse train. The break is magnified by a factor of 5 for visual clarity.

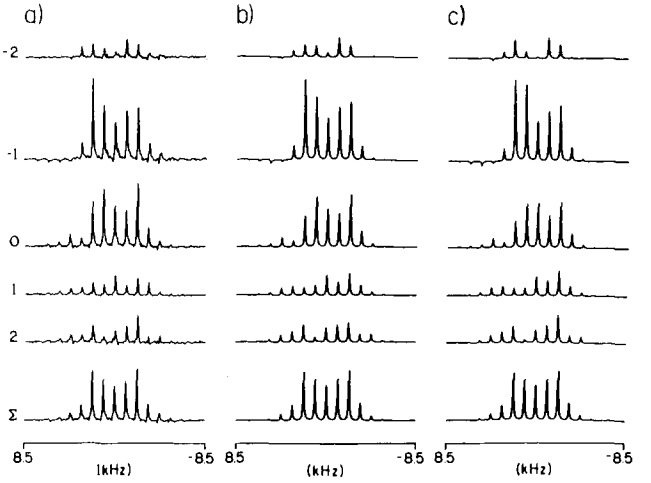

Figure 5. Dipolar cross sections taken from the 2D spectrum shown in Figure 2. Each trace runs parallel to ω_1, through a particular rotational sideband in ω_2. (a) experimental ^{15}N–^{1}H spectra from [^{15}N]acetylvaline, ν_R = 1.07 kHz. The two simulations (b and c) assume two different orientations of the dipolar and chemical shift tensors, (χ = 22°, ψ = 0°) and (χ = 17°, ψ = 0°), respectively, and illustrate the subtle differences in orientation which can be detected in the spectra. The experimental spectra are represented in b.

sidebands in ω_1 and the optimal total evolution time may be estimated from the decay of the dipolar rotational echoes with t_1. Between 64 and 192 values of t_1 are typically used, covering up to ten rotational periods. If a refocusing π-pulse is needed, the interval between t_1 = 0 and t_2 = 0 is fixed at an *even* number of rotational periods ($2n/\nu_R$), and the pulse is applied at n/ν_R as shown in Figure 1.

A sample two-dimensional spectrum for a spin-pair has already been presented in Figure 2. It is usually more convenient, however, to extract only those slices parallel to the ω_1 axis that pass through the resonances along the ω_2 axis. Thus dipolar cross sections are obtained corresponding to the centerband and sidebands of the chemical shift spectrum. No information is lost in this alternative presentation, which is demonstrated in Figure 5, but subsequent analysis of the data is greatly facilitated. The slices are analyzed by methods described elsewhere to yield the dipolar coupling constant D_{IS} and the polar coordinates (χ,ψ) of the unique axis of the dipolar tensor in the principal axis system of the chemical shift tensor.[11] The centerband of the dipolar sum is neglected when D_{IS} is derived, for reasons discussed below.

Results and Discussion

The experimental procedures discussed above were followed for polycrystalline samples of [^{15}N]acetylvaline, α-[^{15}N]glycyl-[^{15}N]glycine, [^{15}N]glycyl[^{15}N]glycine·HCl·H$_2$O, [^{15}N]acetyl-glycine, [π-^{15}N]-1-histidine·HCl·H$_2$O, and [ϵ-^{15}N]tryptophan.

Table I. Summary of NMR Data

compound	σ_{iso}[a]	σ_{11}[b]	σ_{22}[b]	σ_{33}[b]	angles[c] χ	angles[c] ψ	r_{N-H} (Å) NMR[d]	r_{N-H} (Å) neutron
[^{15}N]acetylvaline	81.9	17.2	42.2	186.3	22	0	1.049	
[^{15}N]acetylglycine	74.3	0.5	40.7	181.7	25	0	1.037	
glycylglycine·H_2O								
N–H	77.8	9.2	39.7	184.5	25	0	1.061	1.0200[e]
								1.0240
NH_3*	−12.1							1.0371
glycylglycine·HCl·H_2O								
N–H	72.2	20.0	25.6	171.0			1.063	1.034[f]
	(88.4)	(18.2)	(28.8)	(173.8)				1.038
NH_3*	−3.9							
l-histidine·HCl·H_2O	150.2	32.2	181.5	236.9	90	0	1.093	1.070[g]
		(20.2)	(183.2)	(245.6)				
l-tryptophan·HCl	+89.3	+150.2	+95.6	+22.1	90	0	1.058	0.995[h]
trimethylammonium hydrochloride	−2.9						1.075	
trimethylammonium hydroiodide	+3.2						1.065	

[a] Measured relative to solid $^{15}NH_4Cl$ under MASS; estimated error is ±0.2 ppm. $^{15}NH_4Cl$ (solid) is 14.8 ppm downfield of 5.6 M $^{15}NH_4Cl$ in H_2O. [b] Measured from static powder patterns and/or fitting of rotational sideband intensities as described in the text or from published values (in parentheses). Estimated error is ±3 ppm. [c] The angles relating the heteronuclear dipolar tensor and the ^{15}N chemical shift tensor are obtained from simulations as shown in Figures 4 and 5. χ and ψ are defined in ref 11. Estimated error is ±5°. [d] The NMR bond distances were obtained as described in the text. Estimated error is ±0.065 Å. [e] Kvick, A.; Al-Karaghonli, A. R.; Koetzle, T. F. *Acta Crystallogr.* **1977**, *B33*, 3796. [f] Koetzle, T. F.; Hamilton, W. C.; Parathasgrathy, R. *Acta Crystallogr.* **1972**, *328*, 2083. [g] Fuess, H.; Hohlwein, D.; Mason, S. A. *Acta Crystallogr.* **1977**, *B33*, 654. [h] Koetzle, T. F., private communication. [i] MacKay, M. F. *Cryst. Struct. Comm.* **1975**, *4*, 225.

Results are summarized in Table I, which lists all the parameters needed to describe the dipolar and chemical shift tensors. In each instance the complete experimental protocol was repeated for at least two different rotation rates in order to gauge the precision of the data.

The first four ^{15}N–^1H systems, all peptide linkages, yield similar results. In particular, the unique principal axis of the dipolar tensor in each peptide is rotated approximately 20° from the σ_{zz} principal axis of the chemical shift tensor, which suggests that the geometry of the linkage is nearly identical in the different materials. The location of the other two principal axes cannot be determined accurately in this experiment because of the near axial symmetry of the ^{15}N chemical shift tensor. The ^{15}N–^1H bond distances do vary slightly, and these variations are clearly outside the limits of error of the NMR experiments.

Four of the compounds studied here have also been examined by neutron diffraction methods. A comparison of the ^{15}N–^1H bond lengths and principal axis orientations measured in this work with data obtained from other sources is also given in Table I and is illustrated in Figure 6. Note that the bond distances obtained by NMR correlate well with those obtained by neutron diffraction but are uniformly 0.035 Å longer in both short (~1.06 Å in Gly·Gly·HCl·H_2O) and long (~1.10 Å in l-His·HCl·H_2O) NH bonds. It is worth mentioning here that these distances are consistently shorter than those measured in early dipolar/chemical shift NMR studies from this and other laboratories; for example, in Gly·Gly·HCl·H_2O[12] and in ^{15}N-labeled DNA[14] samples NH bond distances of 1.12 Å were reported. We believe the primary source of this ~0.06 Å difference is the more careful attention paid to the execution of the experiment and particularly the measurement of the heteronuclear scaling factor as described above. The data in Table I and in Figure 6 clearly indicate that these experiments are capable of providing accurate and precise structural information which is otherwise available only from neutron diffraction experiments.

The observation of apparently long bonds with NMR experiments has been noted before and can be attributed to several effects. First, NMR and neutron diffraction differ fundamentally in the time scales of the measurements: NMR events are observed over intervals usually no shorter than tens of microseconds whereas neutron diffraction events require only picoseconds. Consequently, small amplitude libratory or "wagging" motions are averaged over different time scales and therefore can produce discrepancies in the measured bond lengths.[23] In general, rapid librations tend to decrease the dipolar coupling and thus increase the observed bond distance.

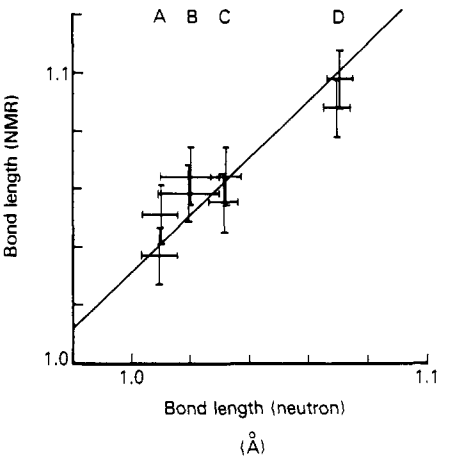

Figure 6. Comparison of ^{15}N–^1H bond distances obtained by solid-state NMR techniques with distances obtained by single-crystal neutron-diffraction techniques. The NMR bond lengths are consistently 0.0035 Å longer than those found by neutron diffraction. In many systems NMR may be the method of choice owing to a lack of suitable single crystals.

Second, NMR and neutron diffraction also differ in the distance function sampled: NMR measures the dipole–dipole interactions, which are proportional to $1/r^3$, but diffraction experiments measure scattering amplitudes, which are proportional to $1/r$. Geometric arguments similar to those above show that NMR further accentuates any apparent shortening of the bond distance when vibrations are averaged over $1/r^3$. Although this distance dependence suggests that NMR should be more sensitive than neutron diffraction to variations in the bond length, the error bars in Figure 6 are approximately equal for both sets of data, owing to additional uncertainties in the NMR experiment.

Other possible reasons for the apparent lengthening of the bond in NMR measurements include variations in the multiple-pulse scaling factor and the contribution of distant protons to the dipolar interaction. As for the scaling factor, measurements made before and immediately after the two-dimensional experiment usually show some variation in this quantity, but not enough to add significantly to the overall error. Of more concern is the validity of approximating the system as an isolated pair of spins in which the nitrogen resonates in the local field of only the directly bonded proton. Fortunately, in all the systems studied the closest nonbonded protons are twice as far from the nitrogen as the directly

(23) Henry, E. R.; Szabo, A. *J. Chem. Phys.* **1985**, *82*, 4753.

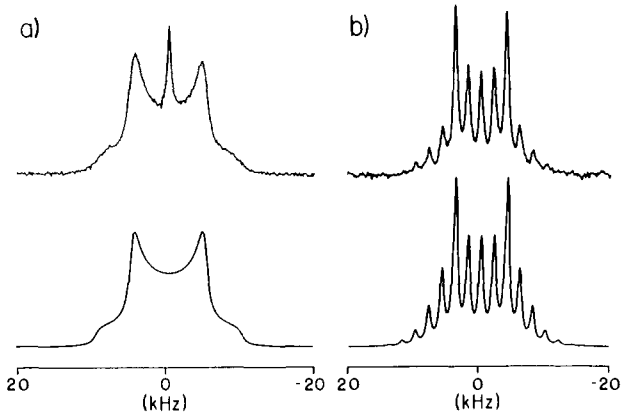

Figure 7. Experimental spectra (top) and theoretical (bottom) ^{1}H-coupled ^{15}N MASS spectra of [^{15}N]trimethylammonium chloride. The ^{15}N chemical shift anisotropy is very small (~8 ppm), so the convolved pattern resembles a dipolar pattern alone. In b ν_R = 1.97 kHz.

bonded proton, so the next-neighbor coupling constants are reduced to approximately 10% of the dominant coupling constant. Sample spinning reduces the effective contribution of the distant interactions even more, for these small couplings are averaged nearly to zero over the period of rotation. To confirm these predictions we simulated each ^{15}N–^{1}H dipolar spectrum with and without up to three next-neighbor protons. The neighboring protons were positioned at coordinates obtained from neutron diffraction studies, and the complete dipolar tensor was calculated for each ^{15}N–^{1}H bond length. In each instance the best value for the bond distance, as determined by a least-squares fit, was the same regardless of the presence of the nonbonded protons.

The neglect of homonuclear proton couplings is justified by the efficient performance of the MREV-8 sequence, which typically reduces the widths of the resonances to 2 ppm or less in ^{1}H multiple-pulse spectra and to 50–100 Hz or less in two-dimensional magic-angle spectra. Nevertheless, it is also possible to perform the local field experiment without incorporating a multiple-pulse line-narrowing sequence into the evolution period. Two alternatives, both of which suffer from disadvantages, are to use a Lee–Goldburg off-resonance spin-lock[24] or to refrain entirely from proton irradiation during t_1.

The Lee–Goldburg method, a continuous wave analogue of the multiple-pulse techniques, relies on the resonance offset due to the ^{1}H chemical shift to contribute a z component to the effective field in the proton rotating frame. The offset is adjusted so that when rf irradiation is applied along the x axis in the rotating frame, the resultant effective field is inclined at the magic angle relative to the z axis. In the presence of this effective field, the spin system appears to be governed only by scaled chemical shift interactions and scaled heteronuclear couplings; homonuclear couplings are averaged to zero. Difficulties arise, however, because the scaling of interactions linear in the angular momentum operator I_z is not uniform over the full range of offsets. The ^{15}N–^{1}H dipolar pattern is inhomogeneously broadened by contributions from crystallites with different orientations and, as a result, extends over several kHz. The resulting variation of the scaling factor over the range of frequency offsets can be as much as 10% even for moderate proton irradiation fields, say 50 kHz. Moreover, the proton resonance offset is modulated by the rotation of the sample, and a simple time average is inappropriate in this instance because the heteronuclear dipolar interaction is modulated simultaneously. By contrast, the multiple-pulse experiment benefits from a scaling factor that is essentially constant over the entire frequency range.

The elimination of all proton irradiation during t_1 removes any uncertainty about the scaling factor and at the same time approximately doubles the breadth of the observed dipolar pattern. Unfortunately, the inevitable increase in the homogeneous dipolar line width, which can approach 10 kHz, usually obscures the important features of the spectrum. In addition, the narrowing power of the magic-angle technique decreases considerably when homonuclear interactions are present.

Failure to irradiate the protons during the dipolar evolution period can lead to complications even when the homogeneous line width is relatively narrow. The one-dimensional static and magic-angle spectra of [^{15}N]trimethylammonium chloride, presented in Figure 7, demonstrate some of the problems. The static dipolar powder spectrum is well simulated as a simple Pake pattern arising from a spin-pair with an internuclear separation of 1.07 Å; chemical shift anisotropy, which is no greater than approximately 8 ppm, contributes only slightly to the line shape. The sharp spike in the middle of the spectrum is presumably due to a small number of molecules dissolved in the water of the hygroscopic material. These molecules execute rapid isotropic motions that average the dipolar coupling nearly to zero. The uncoupled magic-angle sample spinning spectrum, however, is more difficult to analyze quantitatively. First, the rotational sidebands are only partially resolved, so the entire spectrum seems to be sitting on a hump. Second, although the overall appearance of the spectrum is reproduced qualitatively in the simulation, subtle differences are apparent nonetheless, and no single ^{15}N–^{1}H bond distance yields a fully satisfactory result. For example, the outer rotational sidebands are too intense in the simulation shown, which used a value of 1.045 Å to fit the center of the pattern. A simulation using 1.090 Å fits the outer rotational sidebands, but then the center of the simulation is too strong. The least-squares value is 1.065 Å, but the overall quality of the fit is 20–50 times worse than what results from data obtained with the MREV-8 sequence. Even so, we have selected a *favorable* case. These spectra are much better resolved than those obtained from most solids, owing to the motion of the methyl groups and the threefold symmetry about the ^{15}N–^{1}H bond.

Other variations of the local field experiment also exist, and some of these can introduce errors into the bond distance determination. One version of the experiment exploits the periodicity of the internal Hamiltonian under sample rotation by restricting the total dipolar evolution time to one rotational period.[25] The signal obtained in this fashion may either be Fourier transformed immediately or first replicated any number of times to generate a periodic waveform over a longer interval. The practice is justifiable theoretically; in practice most computer programs designed to simulate magic-angle spectra operate in this fashion. Nevertheless, experimental complications often arise. If the multiple-pulse train is functioning poorly, two components with different decay rates may be present during the dipolar evolution period, and bizarre line shapes may be observed. The fast component usually decays in 100–300 μs, somewhat faster than one rotational period, but the slower decay of 3–10 ms more accurately reflects the spin dynamics under the line-narrowing sequence. Hence Fourier transformation of data collected for only one rotational period may distort the dipolar spectrum. The problem is avoided if the dipolar evolution is monitored over 5–10 rotational periods, and if the integrated intensities of the rotational sidebands are used as inputs to the various computer programs.

Conclusions

The high-resolution dipolar/chemical shift experiments performed in this work yield ^{15}N–^{1}H bond distances measurable to 0.005 Å when care is taken to adjust the multiple-pulse line-narrowing sequence and to measure its heteronuclear scaling factor. The bond lengths obtained are consistently 0.035 Å longer than those measured by neutron diffraction techniques, owing mainly to differences in the time scales and distance functions characteristic of the two techniques. The NMR experiment can simultaneously address many sites in a polycrystalline or amorphous sample and provide all the necessary data after only 12–36 h of measuring time. Analysis of the data is undertaken according to methods described in detail here and in earlier papers and requires no more than 5–10 h on a PDP 11/34 minicomputer.

(24) Lee, M.; Goldburg, W. I. *Phys. Rev.* **1965**, *A140*, 1261.

(25) Schaefer, J. F.; Stejskal, E. O.; McKay, R. A.; Dixon, W. T. *Macromolecules* **1984**, *17*, 1479.

The local field experiment is fully applicable to other spin-pairs, including (but not limited to) $^{13}C-^{1}H$, $^{31}P-^{1}H$, and $^{13}C-^{15}N$.

Acknowledgment. This research was supported by the National Institutes of Health (GM-23403, GM-23289, GM-23316, and RR-00995) and by the National Science Foundation through its support of the Francis Bitter National Magnet Laboratory (DMR-8211416). J.E.R. was the recipient of an NIH Postdoctoral Fellowship (GM-09108). We thank T. F. Koetzle for communicating to us the crystallographic data on tryptophan.

Axial Ligation-Induced Structural Changes in Nickel Hydrocorphinoids Related to Coenzyme F_{430} Detected by Raman Difference Spectroscopy†

J. A. Shelnutt

Contribution from the Process Research Division 6254, Sandia National Laboratories, Albuquerque, New Mexico 87185. *Received November 14, 1986*

Abstract: Raman difference spectroscopy provides a structural probe of the state of axial ligation of Ni(II) in nickel corphinoids of the type occurring in coenzyme F_{430} of the methylreductase enzyme of methanogenic bacteria. The two model nickel corphinoids investigated, which have all of the structural features of the natural chromophore, were synthesized by A. Fässler, A. Pfaltz, and A. Eschenmoser (*J. Chem. Soc., Chem. Commun.* **1984**, 1365). Raman lines analogous to the core-size marker lines of metalloporphyrins are identified for the Ni corphinoids, and, just as for the Ni porphyrins, the frequencies for the group of Raman marker lines characterize the 4-, 5-, and 6-coordinate complexes. Further, complexes with two strong nitrogenous bases (e.g., piperidine) can be distinguished from complexes with weak basic ligands (e.g., methanol) on the basis of the frequencies of these Raman lines. Finally, Raman spectra of polycrystalline samples of the Ni corphinoid and its monoisothiocyanate complex show that the structures existing in solution differ markedly from the structures in the crystalline state. The Raman markers will be useful in elucidating the structure of coenzyme F_{430} and its interaction with the nearby protein environment in component C of the methyl-S-coenzyme-M reductase system.

Methylreductase catalyzes the final step in the production of methane from carbon dioxide and hydrogen in methanogenic bacteria.[1,2] Carbon dioxide may be replaced as a substrate in methanogenesis by other small molecules such as methanol, formate, and acetate.[2] The final step in methanogenesis is the two-electron reduction of the methyl group of the intermediate methyl-S-coenzyme M (2-(methylthio)ethanesulfonate)[1] to methane. Methyl-coenzyme M methylreductase from *Methanobacterium thermoautotrophicum* has been purified to homogeneity[3-5] and shown to contain cofactor F_{430}, a nickel-containing tetrapyrrole derivative.[6-8] Recently, the structure **1** of factor F_{430}

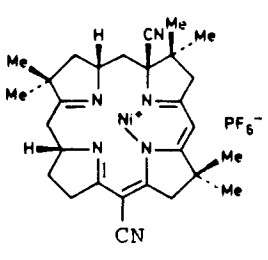

2

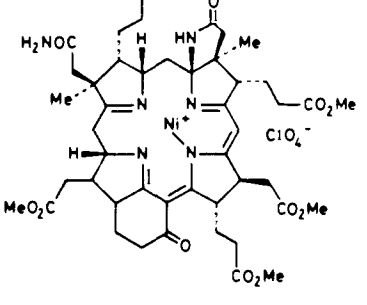

F430M

1

was determined.[9-11] F_{430} is a nickel corphinoid derivative that has all four pyrrole rings reduced. The corphinoid macrocycle incorporates aspects of both the corrins and the porphins in that the molecule has the carbon–nitrogen skeleton of the porphin and the conjugation system found in corrins.[12] Peripheral substitution of the uroporphinoid macrocycle of F_{430} includes two fused rings, one of which connects a β carbon of pyrrole D to the adjacent bridging carbon between pyrroles C and D.

It is important to elucidate the role of F_{430} in the production of methane because biomimetic chemical or photochemical production of methane is a process that has commercial utility as a source of fuels and chemical feedstocks. The mechanism of action of the methylreductase enzyme is also of interest in the area of catalytic C–H bond activation chemistry. Speculation concerning the catalytic function of F_{430} has centered on its pronounced affinity for axial ligands, ruffling of the tetrapyrrole ligand, and the ability of Ni(II) in F_{430} to reversibly reduce to Ni(I).[9-15]

Here, the identification of several structure-sensitive resonance Raman lines that characterize the 4-, 5-, and 6-coordinate com-

† This work performed at Sandia National Laboratories, supported by the U.S. Department of Energy, Contract DE-AC04-76DP00789, and the Gas Research Institute, Contract 5082-260-0767.

(1) Taylor, C. D.; Wolfe, R. S. *J. Biol. Chem.* **1974**, *249*, 4879.
(2) Gunsalus, R. P.; Wolfe, R. S. *Biochem. Biophys. Res. Commun.* **1977**, *76*, 790.
(3) Ellefson, W. L.; Wolfe, R. S. *J. Biol. Chem.* **1981**, *256*, 4259.
(4) Ellefson, W. L.; Whitman, W. B.; Wolfe, R. S. *Proc. Natl. Acad. Sci. U.S.A.* **1982**, *79*, 3707.
(5) Noll, K. M; Rinehart, K. L., Jr.; Tanner, R. S.; Wolfe, R. S. *Proc. Natl. Acad. Sci. U.S.A.* **1986**, *83*, 4238.
(6) Gunsalus, R. P.; Wolfe, R. S. *FEMS Microbiol. Lett.* **1978**, *3*, 191.
(7) Diekert, G.; Klee, B.; Thauer, R. K. *Arch. Microbiol.* **1980**, *124*, 103.
(8) Whitman, W. B.; Wolfe, R. S. *Biochem. Biophys. Res. Commun.* **1980**, *92*, 1196.
(9) Pfaltz, A.; Juan, B.; Fässler, A.; Eschenmoser, A.; Jaenchen, R.; Gilles, H. H.; Diekert, G.; Thauer, R. K. *Helv. Chim. Acta* **1982**, *65*, 828.
(10) Livingston, D. A.; Pfaltz, A.; Schreiber, J.; Eschenmoser, A.; Ankel-Fuchs, D.; Moll, J.; Jaenchen, R.; Thauer, R. K. *Helv. Chim. Acta* **1984**, *67*, 334.
(11) Hausinger, R. P.; Orme-Johnson, W. H.; Walsh, C. *Biochemistry* **1984**, *23*, 801.
(12) Johnson, A. P.; Wehrli, P.; Fletcher, R.; Eschenmoser, A. *Angew. Chem., Int. Ed. Engl.* **1968**, *7*, 623.
(13) Fässler, A.; Pfaltz, A.; Kräutler, B.; Eschenmoser, A. *J. Chem. Soc., Chem. Commun.* **1984**, 1365.
(14) Krafky, C.; Fässler, A.; Pfaltz, A.; Kräutler, B.; Juan, B.; Eschenmoser, A. *J. Chem. Soc., Chem. Commun.* **1984**, 1368.
(15) Jaun, B.; Pfaltz, A. *J. Chem. Soc., Chem. Commun.* **1986**, 1327.

0002-7863/87/1509-4169$01.50/0